

pubs.acs.org/est Article

Persistence and Potential Atmospheric Ramifications of Ice-**Nucleating Particles Released from Thawing Permafrost**

Kevin R. Barry,* Thomas C. J. Hill, Kathryn A. Moore, Thomas A. Douglas, Sonia M. Kreidenweis, Paul J. DeMott, and Jessie M. Creamean

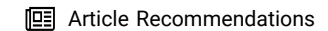


Cite This: Environ. Sci. Technol. 2023, 57, 3505-3515



ACCESS I

Metrics & More



Supporting Information

ABSTRACT: Permafrost underlies approximately a quarter of the Northern Hemisphere and is changing amidst a warming climate. Thawed permafrost can enter water bodies through top-down thaw, thermokarst erosion, and slumping. Recent work revealed that permafrost contains ice-nucleating particles (INPs) with concentrations comparable to midlatitude topsoil. These INPs may impact the surface energy budget of the Arctic by affecting mixedphase clouds, if emitted into the atmosphere. In two 3-4-week experiments, we placed 30,000- and 1000-year-old ice-rich silt permafrost in a tank with artificial freshwater and monitored aerosol INP emissions and water INP concentrations as the water's salinity and temperature were varied to mimic aging and transport of thawed material into seawater. We also tracked aerosol and



water INP composition through thermal treatments and peroxide digestions and bacterial community composition with DNA sequencing. We found that the older permafrost produced the highest and most stable airborne INP concentrations, with levels comparable to desert dust when normalized to particle surface area. Both samples showed that the transfer of INPs to air persisted during simulated transport to the ocean, demonstrating a potential to influence the Arctic INP budget. This suggests an urgent need for quantifying permafrost INP sources and airborne emission mechanisms in climate models.

KEYWORDS: ice-nucleating particles, permafrost, erosion, thermokarst lake, bacteria

1. INTRODUCTION

Recent estimates place the Northern Hemisphere permafrost land coverage at approx. 22% of the exposed land area.1 However, permafrost—earth material like bedrock, soils, and peat that remains at or below 0 °C for two or more years—is thawing across the Arctic because mean annual ground temperatures have been increasing over the past several decades. For example, Burn and Kokelj² found increases of 1.5 °C in the Mackenzie Delta, Canada, between the 1970s and 2007, and globally, the permafrost temperature has increased by 0.29 °C from 2007 to 2016.³ Thermokarst lakes (TKLs), land depressions resulting from the thawing of ice-rich permafrost, are forecast to increase in a warmer climate, exacerbated by an increase in wildfires accelerating thaw. Within permafrost regions, TKLs cover up to 50% of land.⁶ However, TKLs are inherently dynamic due to being susceptible to drainage, and a projected increase of drained area will further alter the Arctic landscape by, for example, promoting a rapid accumulation of peat.7 Additionally, an increased likelihood of coastal erosion from thawing permafrost bluffs poses innumerable economic and environmental challenges, such as damaged infrastructure and ecosystem shifts.

TKLs are vessels for undecomposed carbon from deep permafrost, altering the surface microbial community and leading to greenhouse gas production (methane and carbon dioxide) emitted into the atmosphere through ebullition.^{7,9,10} Permafrost harbors a wide diversity of both anaerobic and aerobic bacteria 11 and contrasts with communities both within and near TKLs, which have been found to be distinct and complex. For example, Ren et al. 12 found a higher bacterial α diversity in thermokarst water than sediment, and Zhou et al. 13 found higher sample richness and evenness in thermokarst pit and headstream samples than in rivers.

Thawed permafrost material entering TKLs and the ocean through coastal erosion or riverine transport can become aerosolized through wave breaking and bubble bursting, forming lake and sea spray aerosols. For example, freshwater whitecaps were found in Lake Michigan at wind speeds greater

September 7, 2022 Received: Revised: February 10, 2023 Accepted: February 13, 2023 Published: February 22, 2023





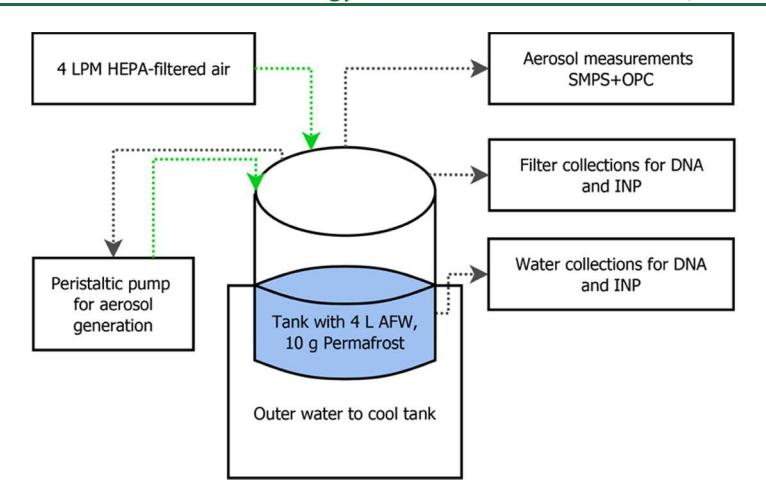




Figure 1. (Left) Diagram showing inputs (green) and outputs (gray) into/from the tank. (Right) Image of the tank running at day 2 with 20,000-year-old permafrost (experimental pretest). The tank body is glass, the lid is stainless steel, and the tank is sealed with a silicone gasket.

Days 1-13	Day 14	Days 15-16	Days 17-25
Artificial Freshwater	Salinity=5.5 g/L	Salinity=17.5 g/L	Salinity=30 g/L
Temperature= 15 °C	Temperature= 9 °C	Temperature= 9 °C	Temperature= 4 °C

Figure 2. Approximate experimental schedule showing tank water salinity and the temperature over time. Conditions were selected to mimic thermokarst lakes (days 1–13), estuaries (days 14–16), and the Arctic Ocean (days 17–25). The color scale used here and in subsequent plots represents the phases of the experiments, defined by increasing salinity and decreasing temperature.

than a modest 3.5 m/s¹⁴ and a quadratic relationship was found between droplet production and wind speed in a simulated freshwater experiment. 15 These lake and sea spray aerosols could be a significant source of ice-nucleating particles (INPs), particles that affect cloud glaciation. INPs are necessary to initiate cloud ice formation at temperatures warmer than the level of homogeneous freezing (-38 °C), and by doing so, they can alter cloud microphysics, radiative properties, and lifetime. 16,17 Despite a diverse range of sources and ice-containing clouds being the dominant source of global precipitation, 20 INPs are atmospherically rare. In the Arctic, land-based INP measurements highlighted a seasonally dependent contribution of terrestrial sources (soil dust, vegetation).^{21–24} Previously, Alaskan permafrost was collected and tested,²⁵ and INP concentrations were found to be similar to midlatitude soil²⁶ and glacial dust.²⁷ The permafrost INPs were predominantly organic with some biological (inferred from heat sensitivity) influence.

An important concern is the potential for INPs from thawed permafrost to affect Arctic mixed-phase clouds (AMPCs), as AMPC persistence and ubiquity across all seasons exert extensive influence on the surface energy budget.²⁸⁻³⁰ AMPC cloud temperatures are commonly between -25 and -5 °C, 29 which is within the range of activity of many INP sources: mineral dust is efficient below about -15 °C, 31 biological material (e.g., bacteria, fungi, plant tissue) initiates freezing up to, and at times warmer than, -5 °C, 18,32 and heat-stable organics (e.g., fractions of soil organic matter) dominate across the temperature spectrum. ^{17,26,33,34} Currently, climate models vary in their representation of Arctic cloud coverage over an annual cycle, likely due to their cloud ice parameterizations.³⁵ INPs are generally poorly represented in models³⁶ but are fundamental to better constrain Arctic amplification, the enhanced high-latitude surface warming.³⁷ Given the potential of thawed permafrost to serve as a reservoir of Arctic INPs, this potential feedback to climate warming must be considered for inclusion in future models. Aerosolization of permafrost material from TKLs during fluvial and estuarine transport and following discharge into the Arctic Ocean, provides pathways for the injection of INPs to the atmosphere. In this study, we build off previous work showing the potential of permafrost to be a notable INP source^{2.5} using tank experiments to simulate the hypothesized transport and aerosolization processes to gain insight into the potential for thawed permafrost to influence AMPCs.

2. MATERIALS AND METHODS

2.1. Tank and Experimental Design. Two separate experiments on permafrost cores were conducted between February and April 2021. Permafrost samples were collected at the Cold Regions Research Laboratory's Permafrost Research Tunnel in Fox, Alaska, and analyzed for their intrinsic INP properties.²⁵ The Tunnel provides access to ice cemented silt representing high carbon content "Yedoma" permafrost that is largely comprised of windblown loess. From regional studies, the climate is estimated to have been 5 to 9 °C colder during the period between 15,000 and 40,000 years when the Tunnel soils were syngenetically frozen. 40-43 A Snow, Ice and Permafrost Research Establishment (SIPRE) auger was used to collect a range of permafrost core ages and likely variable compositions. A 30,000-year-old core was acquired 83 m into the Tunnel (OT83L), and above the Tunnel, a sample of 500-1000-year-old permafrost (based upon a loess deposition rate of 1 mm/year⁴⁴) was collected at the top of the permafrost table, 69 cm below the surface (S69CM).²⁵ Samples were transported frozen in sterile Whirlpak bags to Colorado State University (CSU), where they remained frozen at -20 °C until analysis. These cores were used in the first and second experiments, respectively, and were chosen to span the largest age range from previous work²⁵ for the simulation of permafrost transport and aerosolization. 10 g of each permafrost core (with material gathered from multiple core

locations) was placed into a 9.5 L tank with 4 L of 0.2 μ m filtered artificial freshwater (AFW), with the recipe based on the Arctic tundra lakes sampled in Pienitz et al. (Table S1). The tank was based on a design by May et al. used to generate lake spray aerosol (Figure 1). To isolate the tank from laboratory air, it was fitted with inlets for HEPA- and carbon-filtered air that continuously entered the tank at 4 L min⁻¹ to flush the headspace. Two plunging jets (2.55 mm diameter) driven by a peristaltic pump (Cole-Parmer) periodically generated aerosols through bubble bursting. A magnetic stir bar in the tank ran continuously on a low setting for gentle mixing throughout the course of the experiment, but material was still able to settle (Figure 1).

Each experiment ran for 3-4 weeks (Figure 2), with the second experiment (S69CM) extended to 28 days to hand-stir and resuspend all sediment and retest the water for INPs since it was found visually to contain coarser material. The temperature of the water was controlled with an outer basin connected to a chiller. Tank temperatures and salinities were selected based on previous water temperature and salinity measurements in Arctic tundra lakes, Admiralty Bay, Alaska and the proximate Beaufort and Chukchi Seas. 45,47-49 Salinity was increased (with Brightwell Aquatics NeoMarine Salt) and the water temperature simultaneously decreased in three steps (Figure 2), mimicking changes during the transport of thawed permafrost material from a TKL into the Arctic Ocean through estuaries in late summer. Microbes released through the dissolution of the permafrost samples were allowed to remain in solution and evolve over the course of the experiments. The only additions to the tank were weekly 0.2 μ m filtered AFW (~200 mL) to compensate for initial evaporative and sample collection losses (during AFW conditions only) and sea salts dissolved in 0.2 μ m filtered deionized (DI) water to compensate for later evaporative and collection losses.

2.2. Aerosol Measurement and Collection. Outlets directly off the tank fed headspace air through precleaned polycarbonate filters held in aluminum in-line filter holders (Pall), which collected aerosol for INP and DNA analyses (Whatman Nuclepore track-etched membranes, 47 mm diameter with 0.05 and 0.2 μ m pore size, respectively). All filters had a 10 μ m precleaned backing filter underneath to prevent contamination from the filter holder support mesh. Filters for INP analyses were precleaned with brief ultrasonication in methanol (two 10 s pulses),⁵⁰ and those used for DNA analyses were soaked in 10% hydrogen peroxide (H₂O₂) for 10 min, 51 each followed by rinses with 0.1 μ m filtered DI water. Aerosols were dried with silica gel diffusion driers <30% relative humidity (RH) and then measured with a scanning mobility particle sizer (3080 SMPS, TSI) that sized particles from approximately 10-500 nm and an optical particle counter (OPC, Alphasense OPC-N2) to measure number concentrations of particles with diameters from 0.38 to 17 μ m.

Aerosol filters and water samples for INP and DNA analyses were collected several times throughout the experiments. Aerosol size distributions measured with the SMPS and OPC ran in parallel during INP filter collection periods. During filter collections, the peristaltic pump was turned on (280 mL min⁻¹ per jet) to simulate wave breaking and bubble bursting or heavy rain. Filters for INP analyses were sampled for 2–3 h at a flow rate of about 1.75 standard liters (sL) min⁻¹ (0 °C and 101.325 kPa) to collect approximately 250 sL per filter. DNA filters ran overnight for about 12 h to obtain a greater sample volume for downstream analyses. Both INP and DNA filter

samples were stored in sterile Petri dishes (Pall). At the end of each INP filter period, water samples for both INP and DNA analyses were collected into sterile 50 mL centrifuge tubes (Corning) by briefly disconnecting the peristaltic pump tubing (but leaving the tank sealed). For INPs, approximately 20 mL of water was collected. For DNA, 150 mL was passed through a Sterivex (Millipore) 0.22 μm pore filtering unit. All samples were either stored at $-20~^{\circ}\mathrm{C}$ until processing to avoid degradation of DNA and INPs, or time-permitting, some INP samples were tested fresh (no difference in concentration was found: Figure S1). In periods of nondisturbance, the peristaltic pump ran continuously at the lowest setting to avoid an anaerobic environment forming in the tubing.

2.3. Processing INP Samples. INP concentrations on filters and in water samples were measured with the CSU Ice Spectrometer (IS). The current setup is most recently described in Barry et al. 52 and DeMott et al. 53 Briefly, aerosol filters were resuspended in either 10 or 12 mL of 0.1 μm filtered DI water. Both the aerosol and water samples were dispensed, along with 20-fold dilutions (250 μ L of sample and 4750 μ L of 0.1 μ m filtered DI water), in groups of 32, 50 μ L droplets into 96-well PCR trays (Optimum Ultra, Life Science Products). The trays were placed into aluminum blocks in the IS, cooled at 0.33 °C min⁻¹, and corrected with a corresponding 0.1 μ m filtered DI water negative control. Frozen fractions were converted to cumulative INP concentrations (sL⁻¹ air or mL⁻¹ water),⁵⁴ the former by considering the total volume of air passed through each filter. Undiluted estuarine and seawater samples were corrected for approximate freezing point depressions of 0.4, 1.2, and 2 °C, at respective tank salinities of 5.5, 17.5, and 30 g L⁻¹. All samples were further corrected with a tank blank experiment with samples collected under the same conditions without permafrost. During this tank blank, aerosol and water samples were collected at three time points: artificial freshwater, artificial seawater, and one-week settled artificial seawater. Exponential regressions, with interpolations as needed, were fit to the blank samples to correct corresponding INP concentrations as a function of time and salinity (typically <10% of the original value). 95% confidence intervals were calculated based on Agresti and Coull.55

Treatments on the aerosol and water samples give general INP composition. S6,57 Selected sample suspensions were heated at 95 °C for 20 min to destroy proteinaceous (heatlabile) INPs and digested in 10% $\rm H_2O_2$ under UV-B light and 95 °C heat for 20 min to remove all organic (both heat-labile and -stable) INPs. The INPs remaining after peroxide digestion comprise the inorganic fraction and were presumed to be of mineral origin. Samples from the blank experiment were also put through treatments to produce corrections for the treatment data. Additionally, day 1 water samples for each experiment were passed through 10, 1, and 0.2 μ m pore size filters, using 13 mm diameter polycarbonate filters (Whatman Nuclepore track-etched membranes) for size fractionation of the initial permafrost INPs after their suspension in the tank.

2.4. Processing of DNA Samples. Aerosol samples for DNA analyses were concentrated and extracted following the methods in Uetake et al. For water samples, the Sterivex unit was cracked open with a PVC pipe cutter before the filter resuspension was concentrated, and DNA extracted identically to the aerosol samples. The V4–V5 region of the 16S ribosomal RNA gene was targeted with \$15yF/926pfR primers with Illumina adapters and temperature cycling

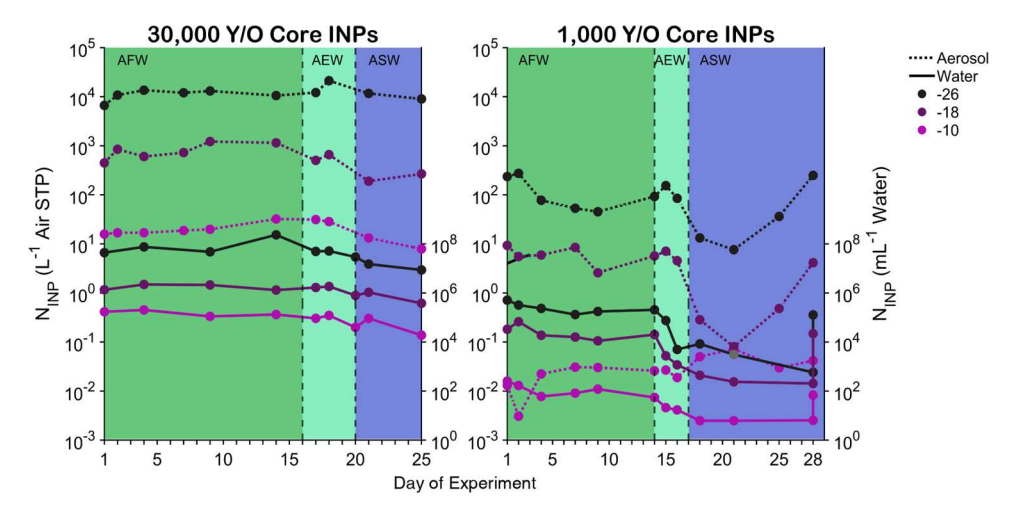


Figure 3. Measured ice-nucleating particle (INP) concentrations for the aerosol (dotted lines: left axes) and water (solid lines: right axes) as a function of experiment day for temperatures of -26 (black), -18 (purple), and -10 °C (magenta). The 30,000-year-old (OT83L) permafrost core experiment is plotted on the left and the 1000-year-old (S69CM) permafrost core experiment on the right. Background shading denotes salinity transitions (AFW = artificial freshwater, AEW = artificial estuary water, ASW = artificial seawater). Filled gray marker for S69CM day 21 water at T = -26 °C is given the value before background correction as the corrected value went below the limit of detection.

conditions identical to Uetake et al.⁵¹ One point of difference is the use of UCP Multiplex PCR master mix (Qiagen), after tests indicated enhanced amplification. After amplification, samples were purified with AMPure XP (Beckman Coulter), barcoded with IDT for Illumina Nextera DNA UD Indexes, and sequenced at the Colorado State University Next Generation Sequencing Core with the Illumina MiSeq Reagent Kit v3 (600-cycle).

Reads were demultiplexed in the Illumina BaseSpace Sequence Hub platform and imported into QIIME2 Version 2021.11⁶⁰ for subsequent analyses. Files were denoised with DADA2 to generate an amplicon sequence variant table. Next, preformatted SILVA 138 reference sequence and taxonomy files were used, and taxonomy was assigned using the QIIME2 feature-classifier plugin. Any mitochondrial, chloroplast, and archaeal reads were removed. Samples were corrected for the tank (2 aerosol and 1 water), 1 concentration and extraction blank, and 2 PCR negative controls with the decontam package prevalence and frequency methods. Lastly, samples were rarefied at approximately 17,000 reads for calculation of diversity metrics.

3. RESULTS AND DISCUSSION

3.1. Temporal Variability of INP Concentrations. Over the course of the experiments, the INPs in the 30,000-year-old (OT83L) and 1000-year-old (S69CM) permafrost had intrinsic differences (Figure 3). The older permafrost had 2-3 orders of magnitude higher INP concentrations compared with the younger permafrost in both the aerosol and water, across all temperatures and salinities. Complete INP temperature spectra are shown in Figures S2 and S3. The INP concentrations from the 30,000-year-old permafrost were relatively constant with time. Notably, there was effectively no change in the aerosol and water INP concentrations for 2 weeks after addition to freshwater. Later, there was a steady but modest decrease when incubated in full seawater. Percent decreases between days 1 and 25 were 40% in the aerosol and 72% in the water at -18 °C. However, INP levels in the water were still elevated, with 400,000 mL⁻¹ at -18 °C on day 25.

Therefore, this type of permafrost material entering TKLs is likely to contribute emissions of INPs for several weeks.

The 1000-year-old permafrost had larger INP decreases overall between days 1 and 25, with 95 and 85% reductions at −18 and −26 °C, respectively, in the aerosol. In the water, decreases between days 1 and 25 were >99% at -10, -18, and -26 °C. In contrast to the older permafrost, salinity had an immediate effect on the younger permafrost, as concentrations dropped shortly after the salt was increased. For example, INPs in the water went from 200,000 to 5000 mL⁻¹ at -26 °C, a 97.5% decrease in 2 days (days 14-16 when salt was increased to 17.5 g L⁻¹). However, this change was somewhat temperature (i.e., INP activation)-dependent, with a decrease of 68% at -10 °C within the same period. The lower INP concentrations, compared to the 30,000-year-old permafrost, combined with a large effect of salinity, suggests a reduced influence of this type of permafrost material on atmospheric INP concentrations.

To test if the rapid decrease of INPs with increasing salinity in the 1000-year-old permafrost was caused by their deactivation or by settling, the tank was hand-stirred on day 28 to resuspend all sediment and retested immediately (Figures 3 and S3). INPs increased in both the aerosol and water across the entire temperature spectrum, rebounding to the original levels measured in artificial freshwater. Thus, the majority of the INP decrease is attributed to sedimentation (of larger INPs: Section 3.2), although flocculation and other unknown mechanisms cannot be ruled out (with some unexpected variability in the aerosol under full salt conditions). Overall, the INP concentrations from the 30,000-year-old permafrost were much more constant with time and salinity than those from the 1000-year-old permafrost, as evidenced by a lower slope of the INP concentration with time in both the aerosol and water (Figure S4).

3.2. Permafrost INP Composition. To investigate reasons for INP concentration differences between the experiments, we next examine their size and composition. The 1000-year-old permafrost contained coarser material and the water in the tank was visually clearer throughout the experiment compared with the 30,000-year-old permafrost.

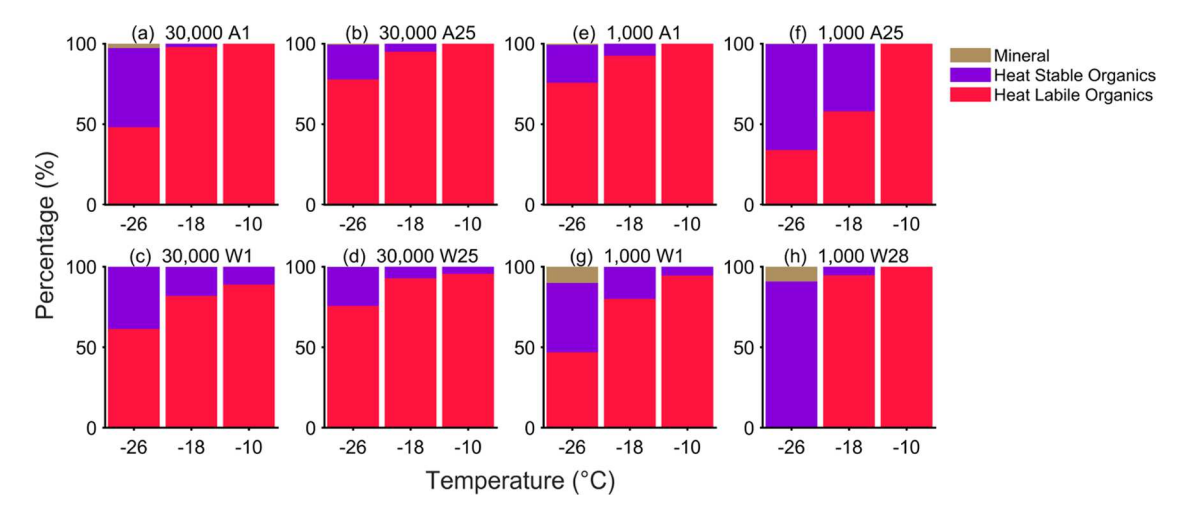


Figure 4. Ice-nucleating particle (INP) compositional histograms for the 30,000-year-old (OT83L: (a–d)) and 1,000-year-old (S69CM: (e-h)) permafrost core experiments from the treatment analyses. The sample type [aerosol (A) or water (W)] and day of experiment are denoted in each plot title. Heat-labile organics (INPs destroyed after 95 °C heating) are in red, heat-stable organics (INPs additionally destroyed after hydrogen peroxide digestion) are in purple, and the remainders (presumed mineral INPs) are shown in tan.

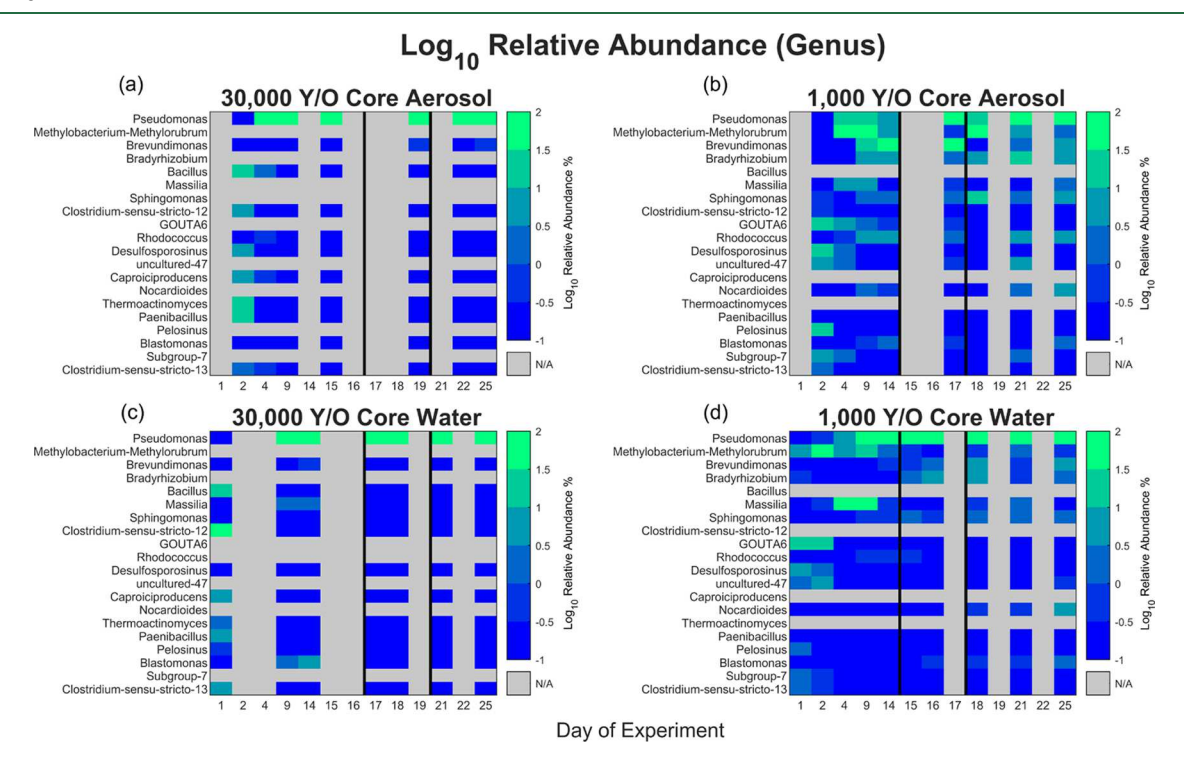


Figure 5. Genus-level relative abundance heatmaps for the aerosol (a, b) and water (c, d) bacterial community for the 30,000-year-old (OT83L: (a, c)) and 1000-year-old (S69CM: (b, d)) permafrost core experiments. The top 20 abundant taxa for the combined dataset are given from top to bottom on the *y*-axis, with the color bar referring to units of log base 10 of the relative abundance percentage. Gray indicates taxa comprising less than 0.1% relative abundance (*y*-axis) or samples not collected on a particular day (*x*-axis). Black lines indicate tank transitions to estuarine (first) or full salt (second) conditions.

Size filtration of the day 1 water indicated that INPs larger than 10 μ m accounted for 60% of the total down to -15 °C of the 1000-year-old core experiment (Figure S5). The younger permafrost also had a bimodal INP population in the water at colder temperatures, with the majority larger than 1 μ m or smaller than 0.2 μ m (e.g., combined 89% at -25 °C), whereas the INPs in the older permafrost were predominantly between 0.2 and 10 μ m (e.g., 89% at -25 °C; 97% at -15 °C). Heat and peroxide treatments on the starting and ending aerosol and water samples for the two experiments revealed that nearly all of the INPs were organic compounds (Figures 4, S6, and S7).

Mineral INPs were only detected at the coldest temperatures (i.e., \sim 3% mineral in the day 1 30,000-year-old permafrost aerosol and 10% mineral in the days 1 and 28 1000-year-old permafrost water at -26 °C). The largest percentage of heat-labile organics was at the warmer temperatures, consistent with the results in Creamean et al.;²⁵ however, they contrastingly always predominated to -20 °C and were sometimes colder than -25 °C. The fraction of heat-labile and heat-stable organics changed with time and between experiments but was also temperature-dependent. For example, in the 1000-year-old permafrost day 1 water, about 50% of the INPs at -26 °C were

heat-labile, while there were no detectable heat-labile INPs at the same temperature by day 28. At the same time, heat-labile INP fractions at -18 and -10 °C increased with time. In the 30,000-year-old permafrost, the compositional changes were more gradual, with a general trend of increased heat-labile INP fractions over time in both the air and water. This may help to explain the greater variability of INP concentrations with time in the younger core (Figures 3 and S4). In both permafrost samples, organic INPs dominated in both the aerosol and water across the temperature spectrum for the range relevant to AMPCs (-25 to -5°C^{29}).

To confirm if the decreases in INPs in the 1000-year-old permafrost were predominately due to sedimentation, treatments were done on the post-stir day 28 water to investigate compositional changes pre- and post-stirring (Figure S8). In the warmer temperature bins (-18 and -10 °C), the post-stirring fractions were almost identical to the day 1 water. However, for the coldest bin (-26 °C), the fractional contributions were more similar to the day 28 prestir sample than to day 1. This indicates that, in addition to INP sedimentation, there were compositional changes over time at colder temperatures, with a permanent loss of a heat-labile population. However, this compositional change did not seem to influence the overall INP concentrations (Figure 3), which suggests a diverse range of INP sources derived from thawed permafrost.

3.3. Compositional and Temporal Variability of the Bacterial Community. With both permafrost core experiments exhibiting differences in INP concentration and composition and a large fraction of INPs in all experiments identified as heat-labile and therefore likely of biological origin, we next explore the bacterial community composition. The aerosol and water genus-level relative abundance heatmaps (Figure 5) show that the bacterial community varied in time and between experiments. The initial compositions were similar to previous permafrost profiles at the phylum level, 67 with the 30,000-year-old permafrost containing a majority of Firmicutes (89%), while the 1000-year-old permafrost contained a mixture of Firmicutes, Chloroflexi, Acidobacteriota, Actinobacteriota, and Proteobacteria.

As the experiments progressed, the 30,000-year-old permafrost was rapidly dominated by fewer taxa, and after the salt was added on day 16, the water and aerosol contained virtually only *Pseudomonas*. The 1000-year-old permafrost also contained a high relative percentage of *Pseudomonas* that increased with time; however, a greater number of taxa codominated compared with the older core, even after the salt was added, and there was more temporal variability. *Pseudomonas* was likely present in low levels in the original permafrost samples, as only six of the 209 *Pseudomonas* amplicon sequence variants (ASVs) were detected in the tank water control (0 detected in the tank aerosol, extraction, and PCR controls); these six may have been carried over since the tank blank experiment was performed last. Additionally, the dominant *Pseudomonas* ASVs varied between experiments.

The trends in the heatmaps are consistent with the aerosol and water α diversities (Figure S9), with a lower Shannon index in the older versus younger core throughout the entire period, ⁶⁸ consistent with previous studies (e.g., Mackelprang et al. ⁶⁹). A Kruskal–Wallis test confirmed the α diversities of the two experiments were significantly different between the aerosol (p=0.02) and water (p=0.04) samples. Within experiments, a p value of 0.03 was found between the aerosol

and water in the 1000-year-old permafrost, but no significance was found between the aerosol and water in the 30,000-year-old permafrost (p = 0.57). A higher α diversity in the aerosol than that in the water in the younger core (Figure S9) shows that the taxa came out of the water in different relative proportions under the disturbance of simulated wave breaking. However, this same trend was not found in the older permafrost, which may be a property of its lower α diversity.

pubs.acs.org/est

In both experiments, the α diversity changed rapidly over the first few days and then stabilized, which was expected as a consequence of placing diverse communities specialized for cold environments into a warm and homogeneous aerobic environment. A comparable attenuation was seen by Zhou et al., 13 who found significantly lower sample richness and evenness in river versus thermokarst pit and headstream samples. However, the relative stabilization in diversity over several weeks was maintained under changing salinity, despite a changing community composition (most pronounced in the younger permafrost). The higher α diversity in the younger permafrost along with greater temporal fluctuations in bacterial community composition are consistent with its larger INP variability, in both number and composition, compared with the older permafrost (Figures 3, 4, and S4), although this method can only serve as a proxy for trends in ice-nucleating bacteria.

3.4. Broader Atmospheric Implications. Both experiments showed variability in the INPs and bacterial community in time and between permafrost cores, but to compare these findings to other known INP sources, a normalization basis is needed, such as the surface active site density parameter $(n_s)^{.70,71}$ This parameter normalizes aerosol INP concentrations by the total aerosol surface area and has been commonly used to describe local and global INP sources such as mineral dust,⁷² clean marine air,⁵⁷ and wildfire smoke.⁵² Here, we assume that all aerosolized particles and INPs are solely from permafrost material exiting a water body and use the measured aerosol size distributions and an assumption of particle sphericity to compute particle surface areas. Figure 6 reveals a wide variability of the n_s parameter spanning over 5 orders of magnitude, with the 30,000-year-old permafrost

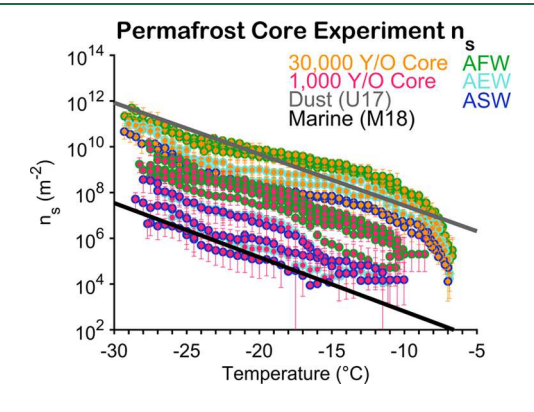


Figure 6. Ice-nucleating particle (INP) surface active site density (n_s) spectra for all aerosol samples from the 30,000-year-old (OT83L: orange) and 1000-year-old (S69CM: pink) permafrost core experiments. Green outlined markers indicate emissions from artificial freshwater (AFW), light blue outlined markers indicate emissions from artificial estuary water (AEW), and dark blue outlined markers indicate emissions from artificial seawater (ASW). Previous parameterizations for desert dust⁷³ and clean marine air⁵⁷ are given in gray and black, respectively.

having larger n_s values overall (significant at 95% confidence across entire temperature spectrum). For reference, previous parameterizations from laboratory-generated desert dust⁷³ and clean marine air⁵⁷ are plotted. This large range is attributed to a decrease of INPs with time for both cores combined with increased emissions of total aerosol (Figures S10 and S11) with salinity (for example, in the 30,000-year-old permafrost, the total surface area increased from 150 to 2500 μ m² between days 1 and 25). The elevated aerosol concentrations with salinity are consistent with May et al. 46 who found a positive relationship between aerosol concentration, bubble number, and ion solution concentration among freshwater and seawater and Zinke et al. 74 who found an increased particle surface area with salinity. A decreased tank temperature could have also contributed to increased aerosol with time during periods with temperatures below 10 °C (when the salts were added).^{74,75} The n_s values from the 30,000-year-old permafrost indicate activity near to or exceeding the desert dust parameterization, which is considered a dominant source of INPs below approximately -15 °C.31 Overall, the 30,000-year-old permafrost contained more INPs per surface area of emitted material than the 1000-year-old permafrost. The 1000-year-old permafrost also had more variable n_s values that coincide with its fluctuating INP concentrations and bacterial community composition. Nonetheless, most values for the younger core (including under oceanic salinity) and all values for the older core were higher than the clean marine air mass parameterization across all temperatures. This suggests that thawed permafrost material could enhance INP emissions in estuarine and sea spray aerosol, despite reductions from INP sedimentation and dilution due to greater aerosol concentrations generated by seawater (than freshwater). However, investigation of the true atmospheric emission rates and potential impacts require considerable future field, lab, and modeling efforts.

Given their high n_s values, aerosolized INPs from thawed permafrost material entering thermokarst lakes, rivers, and oceans have the potential to be a source of atmospheric INPs, but their importance is dependent upon release into and from water bodies through wave breaking and bubble bursting. Potential release mechanisms include top-down permafrost thaw, slope failure (e.g., retrogressive thaw slumping, activelayer detachment slides), and coastal and riverbank erosion. Top-down permafrost thaw is increasing as global permafrost temperatures rise³ and from the conversion between bedfast and floating lakes (those which do not freeze all the way down). Climate warming is leading to the formation of taliks that consist of a year-round thawed zone. 10 Retrogressive thaw slumping is a prodigious source of particulate organic matter that can enter water bodies⁷⁶ and is projected to increase with an increase in rainfall.⁷⁷ Active-layer detachment slides, through which the top layer of the soil becomes detached from the underlying permafrost, can exacerbate permafrost thaw and be an additional source of organic matter to water bodies.⁷⁸ Permafrost coastal erosion and riverbank retreat are also likely to increase in the future, 8,79 especially with ice-rich Yedoma permafrost similar to our core samples, with a higher ice content being more prone to erosion. For example, Kanevskiy et al. 80 found an average retreat of a riverbank in northern Alaska of 11 m per year over 15 years of monitoring. All of these pathways could be sources of INP-rich organic material into water bodies, which may be subsequently emitted into the atmosphere through disturbances. Thawed permafrost material that does not enter water bodies may be an episodic source of INPs to the atmosphere with wind exposure, but we hypothesize that the primary mechanism is through wave breaking and bubble bursting.

Previous work showed that the tested permafrost cores had ice nucleation abilities comparable to glacial soil dust²⁷ and midlatitude soil,²⁶ which means a large potential reservoir of INPs that could be released under a warming climate.²⁵ If the INPs did not become aerosolized, the INP source to the atmosphere would be negligible. For example, the ice nucleation ability of Arizona Test Dust degrades rapidly with only 2 days of aging in deionized water.81 However, in this small-scale laboratory study, we were able to confirm the ability of thawed permafrost INPs to both persist in suspension and enter the atmosphere. When portions of a 30,000-year-old and 1000-year-old permafrost core were placed into a tank with artificial freshwater and subjected to a simulated disturbance, the aerosol INP concentrations were elevated, with those of the older core approaching levels of pure desert dust on a surface area basis.

Even though both permafrost cores showed a potential source of atmospheric INPs, they had fundamentally different properties. Compared with the ancient permafrost, the 1000year-old permafrost had lower and more variable INP concentrations, coarser material with many INPs greater than 10 μ m in the water (susceptible to sedimentation), and a higher bacterial community α diversity. The INPs that sediment out may, however, be periodically resuspended by storms (average of 12-22 stormy days per year in the Arctic Ocean near Alaska⁸²), which can additionally incorporate sediment in sea ice. 83 For example, Inoue et al. 84 found an order of magnitude increase in INPs in the Chukchi Sea under stormy conditions with high turbidity. Compositionally, both permafrost samples had INPs that were nearly all organic across the temperature spectrum, but the younger core was more variable in the heat-labile versus heat-stable fractions over time. The temporal bacterial community composition shifts confirm that thawed permafrost is a dynamic substrate, though the INP populations, especially of the older permafrost, were more resistant to change. More data are needed for model parameterizations, which will not only depend on the type of permafrost but also the water type and likelihood of mixing. Since thawed permafrost INPs have the potential to alter the regional Arctic INP budget and longevity of Arctic mixed-phase clouds, further investigation is of utmost importance under a warmer climate. Overall, the atmospheric implications could extend far beyond the thermokarst lake or coastline from which the thawed material enters the water.

ASSOCIATED CONTENT

Supporting Information

The Supporting Information is available free of charge at https://pubs.acs.org/doi/10.1021/acs.est.2c06530.

Recipe used to make up the artifical freshwater for the tank experiments; fresh versus frozen sample comparison; complete ice-nucleating particle (INP) temperature spectra for the aerosol and water; temporal slope of the INP concentrations; INP size filtration histogram; INP treatment spectra and additional histogram; α diversity plot; aerosol surface area size distributions (PDF)

AUTHOR INFORMATION

Corresponding Author

Kevin R. Barry — Department of Atmospheric Science, Colorado State University, Fort Collins, Colorado 80523-1371, United States; ⊚ orcid.org/0000-0002-1896-1921; Email: kevin.barry@colostate.edu

Authors

- Thomas C. J. Hill Department of Atmospheric Science, Colorado State University, Fort Collins, Colorado 80523-1371, United States; orcid.org/0000-0002-5293-3959
- Kathryn A. Moore Department of Atmospheric Science, Colorado State University, Fort Collins, Colorado 80523-1371, United States; orcid.org/0000-0002-9242-5422
- Thomas A. Douglas U.S. Army Cold Regions Research and Engineering Laboratory, Fort Wainwright, Alaska 99703, United States; orcid.org/0000-0003-1314-1905
- Sonia M. Kreidenweis Department of Atmospheric Science, Colorado State University, Fort Collins, Colorado 80523-1371, United States
- Paul J. DeMott Department of Atmospheric Science, Colorado State University, Fort Collins, Colorado 80523-1371, United States
- Jessie M. Creamean Department of Atmospheric Science, Colorado State University, Fort Collins, Colorado 80523-1371, United States

Complete contact information is available at: https://pubs.acs.org/10.1021/acs.est.2c06530

Notes

The authors declare no competing financial interest.

ACKNOWLEDGMENTS

This work was supported by the National Science Foundation, Award No. 1946657. Kathryn Moore acknowledges support by a National Science Foundation Graduate Research Fellowship under Grant No. 006784. Thomas Douglas acknowledges the US Army Futures Command and the Assistant Secretary for the Army Acquisition, Logistics, and Technology Basic and Applied Research programs. Special thanks to Jun Uetake (now at the National Institute of Polar Research, Tachikawa, Tokyo 190-8518, Japan) for help in sample collection of the 1000-year-old core. We greatly thank the work of two anonymous reviewers for improving this manuscript.

■ REFERENCES

- (1) Obu, J.; Westermann, S.; Bartsch, A.; Berdnikov, N.; Christiansen, H. H.; Dashtseren, A.; Delaloye, R.; Elberling, B.; Etzelmüller, B.; Kholodov, A.; Khomutov, A.; Kääb, A.; Leibman, M. O.; Lewkowicz, A. G.; Panda, S. K.; Romanovsky, V.; Way, R. G.; Westergaard-Nielsen, A.; Wu, T.; Yamkhin, J.; Zou, D. Northern Hemisphere Permafrost Map Based on TTOP Modelling for 2000–2016 at 1 Km2 Scale. *Earth-Sci. Rev.* 2019, 193, 299–316.
- (2) Burn, C. R.; Kokelj, S. V. The Environment and Permafrost of the Mackenzie Delta Area. *Permafrost Periglac. Process.* **2009**, *20*, 83–105.
- (3) Biskaborn, B. K.; Smith, S. L.; Noetzli, J.; Matthes, H.; Vieira, G.; Streletskiy, D. A.; Schoeneich, P.; Romanovsky, V. E.; Lewkowicz, A. G.; Abramov, A.; Allard, M.; Boike, J.; Cable, W. L.; Christiansen, H. H.; Delaloye, R.; Diekmann, B.; Drozdov, D.; Etzelmüller, B.; Grosse, G.; Guglielmin, M.; Ingeman-Nielsen, T.; Isaksen, K.; Ishikawa, M.; Johansson, M.; Johansson, H.; Joo, A.; Kaverin, D.; Kholodov, A.; Konstantinov, P.; Kröger, T.; Lambiel, C.; Lanckman, J.-P.; Luo, D.; Malkova, G.; Meiklejohn, I.; Moskalenko, N.; Oliva, M.; Phillips, M.;

- Ramos, M.; Sannel, A. B. K.; Sergeev, D.; Seybold, C.; Skryabin, P.; Vasiliev, A.; Wu, Q.; Yoshikawa, K.; Zheleznyak, M.; Lantuit, H. Permafrost Is Warming at a Global Scale. *Nat. Commun.* **2019**, *10*, No. 264.
- (4) Luo, J.; Niu, F.; Lin, Z.; Liu, M.; Yin, G. Thermokarst Lake Changes between 1969 and 2010 in the Beilu River Basin, Qinghai—Tibet Plateau, China. *Sci. Bull.* **2015**, *60*, 556–564.
- (5) Chen, Y.; Lara, M. J.; Jones, B. M.; Frost, G. V.; Hu, F. S. Thermokarst Acceleration in Arctic Tundra Driven by Climate Change and Fire Disturbance. *One Earth* **2021**, *4*, 1718–1729.
- (6) Kokelj, S. V.; Jorgenson, M. T. Advances in Thermokarst Research: Recent Advances in Research Investigating Thermokarst Processes. *Permafrost Periglac. Process.* **2013**, *24*, 108–119.
- (7) Jones, B. M.; Grosse, G.; Farquharson, L. M.; Roy-Léveillée, P.; Veremeeva, A.; Kanevskiy, M. Z.; Gaglioti, B. V.; Breen, A. L.; Parsekian, A. D.; Ulrich, M.; Hinkel, K. M. Lake and Drained Lake Basin Systems in Lowland Permafrost Regions. *Nat. Rev. Earth Environ.* 2022, 3, 85–98.
- (8) Irrgang, A. M.; Bendixen, M.; Farquharson, L. M.; Baranskaya, A. V.; Erikson, L. H.; Gibbs, A. E.; Ogorodov, S. A.; Overduin, P. P.; Lantuit, H.; Grigoriev, M. N.; Jones, B. M. Drivers, Dynamics and Impacts of Changing Arctic Coasts. *Nat. Rev. Earth Environ.* **2022**, *3*, 39–54.
- (9) Walter, K. M.; Zimov, S. A.; Chanton, J. P.; Verbyla, D.; Chapin, F. S. Methane Bubbling from Siberian Thaw Lakes as a Positive Feedback to Climate Warming. *Nature* **2006**, *443*, 71–75.
- (10) in't Zandt, M. H.; Liebner, S.; Welte, C. U. Roles of Thermokarst Lakes in a Warming World. *Trends Microbiol.* **2020**, 28, 769–779.
- (11) Ottoni, J. R.; de Oliveira, V. M.; Passarini, M. R. Z. Microbes in Thawing Permafrost: Contributions to Climate Change. In *Microbiome Under Changing Climate*; Elsevier, 2022; pp 1–28.
- (12) Ren, Z.; Zhang, C.; Li, X.; Ma, K.; Cui, B. Abundant and Rare Bacterial Taxa Structuring Differently in Sediment and Water in Thermokarst Lakes in the Yellow River Source Area, Qinghai-Tibet Plateau. *Front. Microbiol.* **2022**, *13*, No. 774514.
- (13) Zhou, L.; Zhou, Y.; Yao, X.; Cai, J.; Liu, X.; Tang, X.; Zhang, Y.; Jang, K.-S.; Jeppesen, E. Decreasing Diversity of Rare Bacterial Subcommunities Relates to Dissolved Organic Matter along Permafrost Thawing Gradients. *Environ. Int.* **2020**, *134*, No. 105330.
- (14) Slade, J. H.; VanReken, T. M.; Mwaniki, G. R.; Bertman, S.; Stirm, B.; Shepson, P. B. Aerosol Production from the Surface of the Great Lakes. *Geophys. Res. Lett.* **2010**, *37*, No. L18807.
- (15) Pietsch, R. B.; Grothe, H.; Hanlon, R.; Powers, C. W.; Jung, S.; Ross, S. D.; Schmale, D. G., III Wind-Driven Spume Droplet Production and the Transport of *Pseudomonas Syringae* from Aquatic Environments. *PeerJ* **2018**, *6*, No. e5663.
- (16) DeMott, P. J.; Prenni, A. J.; Liu, X.; Kreidenweis, S. M.; Petters, M. D.; Twohy, C. H.; Richardson, M. S.; Eidhammer, T.; Rogers, D. C. Predicting Global Atmospheric Ice Nuclei Distributions and Their Impacts on Climate. *Proc. Natl. Acad. Sci. U.S.A.* **2010**, *107*, 11217–11222.
- (17) Kanji, Z. A.; Ladino, L. A.; Wex, H.; Boose, Y.; Burkert-Kohn, M.; Cziczo, D. J.; Krämer, M. Overview of Ice Nucleating Particles. *Meteorol. Monogr.* **2017**, *58*, 1.1–1.33.
- (18) Hill, T. C. J.; DeMott, P. J.; Conen, F.; Möhler, O. Impacts of Bioaerosols on Atmospheric Ice Nucleation Processes. In *Microbiology of Aerosols*; Delort, A.-M.; Amato, P., Eds.; John Wiley & Sons, 2018; pp 197–219.
- (19) Šantl-Temkiv, T.; Sikoparija, B.; Maki, T.; Carotenuto, F.; Amato, P.; Yao, M.; Morris, C. E.; Schnell, R.; Jaenicke, R.; Pöhlker, C.; DeMott, P. J.; Hill, T. C. J.; Huffman, J. A. Bioaerosol Field Measurements: Challenges and Perspectives in Outdoor Studies. *Aerosol Sci. Technol.* **2020**, *54*, 520–546.
- (20) Mülmenstädt, J.; Sourdeval, O.; Delanoë, J.; Quaas, J. Frequency of occurrence of rain from liquid-, mixed-, and ice-phase clouds derived from A-Train satellite retrievals. *Geophys. Res. Lett.* **2015**, 42, 6502–6509.

- (21) Creamean, J. M.; Kirpes, R. M.; Pratt, K. A.; Spada, N. J.; Maahn, M.; de Boer, G.; Schnell, R. C.; China, S. Marine and Terrestrial Influences on Ice Nucleating Particles during Continuous Springtime Measurements in an Arctic Oilfield Location. *Atmos. Chem. Phys.* **2018**, *18*, 18023–18042.
- (22) Si, M.; Irish, V. E.; Mason, R. H.; Vergara-Temprado, J.; Hanna, S. J.; Ladino, L. A.; Yakobi-Hancock, J. D.; Schiller, C. L.; Wentzell, J. J. B.; Abbatt, J. P. D.; Carslaw, K. S.; Murray, B. J.; Bertram, A. K. Ice-Nucleating Ability of Aerosol Particles and Possible Sources at Three Coastal Marine Sites. *Atmos. Chem. Phys.* **2018**, *18*, 15669–15685.
- (23) Santl-Temkiv, T.; Lange, R.; Beddows, D.; Rauter, U.; Pilgaard, S.; Dall'Osto, M.; Gunde-Cimerman, N.; Massling, A.; Wex, H. Biogenic Sources of Ice Nucleating Particles at the High Arctic Site Villum Research Station. *Environ. Sci. Technol.* **2019**, *53*, 10580–10590.
- (24) Wex, H.; Huang, L.; Zhang, W.; Hung, H.; Traversi, R.; Becagli, S.; Sheesley, R. J.; Moffett, C. E.; Barrett, T. E.; Bossi, R.; Skov, H.; Hünerbein, A.; Lubitz, J.; Löffler, M.; Linke, O.; Hartmann, M.; Herenz, P.; Stratmann, F. Annual Variability of Ice-Nucleating Particle Concentrations at Different Arctic Locations. *Atmos. Chem. Phys.* 2019, 19, 5293–5311.
- (25) Creamean, J. M.; Hill, T. C. J.; DeMott, P. J.; Uetake, J.; Kreidenweis, S.; Douglas, T. A. Thawing Permafrost: An Overlooked Source of Seeds for Arctic Cloud Formation. *Environ. Res. Lett.* **2020**, *15*, No. 084022.
- (26) Hill, T. C. J.; DeMott, P. J.; Tobo, Y.; Fröhlich-Nowoisky, J.; Moffett, B. F.; Franc, G. D.; Kreidenweis, S. M. Sources of Organic Ice Nucleating Particles in Soils. *Atmos. Chem. Phys.* **2016**, *16*, 7195–7211.
- (27) Tobo, Y.; Adachi, K.; DeMott, P. J.; Hill, T. C. J.; Hamilton, D. S.; Mahowald, N. M.; Nagatsuka, N.; Ohata, S.; Uetake, J.; Kondo, Y.; Koike, M. Glacially Sourced Dust as a Potentially Significant Source of Ice Nucleating Particles. *Nat. Geosci.* **2019**, *12*, 253–258.
- (28) Intrieri, J. M. An Annual Cycle of Arctic Surface Cloud Forcing at SHEBA. J. Geophys. Res. 2002, 107, No. 8039.
- (29) Shupe, M. D.; Matrosov, S. Y.; Uttal, T. Arctic Mixed-Phase Cloud Properties Derived from Surface-Based Sensors at SHEBA. *J. Atmos. Sci.* **2006**, *63*, 697–711.
- (30) Morrison, H.; de Boer, G.; Feingold, G.; Harrington, J.; Shupe, M. D.; Sulia, K. Resilience of Persistent Arctic Mixed-Phase Clouds. *Nat. Geosci.* **2012**, *5*, 11–17.
- (31) Murray, B. J.; O'Sullivan, D.; Atkinson, J. D.; Webb, M. E. Ice Nucleation by Particles Immersed in Supercooled Cloud Droplets. *Chem. Soc. Rev.* **2012**, *41*, 6519.
- (32) Huang, S.; Hu, W.; Chen, J.; Wu, Z.; Zhang, D.; Fu, P. Overview of Biological Ice Nucleating Particles in the Atmosphere. *Environ. Int.* **2021**, *146*, No. 106197.
- (33) Tobo, Y.; DeMott, P. J.; Hill, T. C. J.; Prenni, A. J.; Swoboda-Colberg, N. G.; Franc, G. D.; Kreidenweis, S. M. Organic Matter Matters for Ice Nuclei of Agricultural Soil Origin. *Atmos. Chem. Phys.* **2014**, *14*, 8521–8531.
- (34) Testa, B.; Hill, T. C. J.; Marsden, N. A.; Barry, K. R.; Hume, C. C.; Bian, Q.; Uetake, J.; Hare, H.; Perkins, R. J.; Möhler, O.; Kreidenweis, S. M.; DeMott, P. J. Ice Nucleating Particle Connections to Regional Argentinian Land Surface Emissions and Weather During the Cloud, Aerosol, and Complex Terrain Interactions Experiment. J. Geophys. Res.: Atmos. 2021, 126, No. e2021JD035186.
- (35) Taylor, P. C.; Boeke, R. C.; Li, Y.; Thompson, D. W. J. Arctic Cloud Annual Cycle Biases in Climate Models. *Atmos. Chem. Phys.* **2019**, *19*, 8759–8782.
- (36) Murray, B. J.; Carslaw, K. S.; Field, P. R. Opinion: Cloud-Phase Climate Feedback and the Importance of Ice-Nucleating Particles. *Atmos. Chem. Phys.* **2021**, *21*, 665–679.
- (37) Tan, I.; Barahona, D.; Coopman, Q. Potential Link Between Ice Nucleation and Climate Model Spread in Arctic Amplification. *Geophys. Res. Lett.* **2022**, *49*, No. e2021GL097373.
- (38) Douglas, T. A.; Mellon, M. T. Sublimation of Terrestrial Permafrost and the Implications for Ice-Loss Processes on Mars. *Nat. Commun.* **2019**, *10*, No. 1716.

- (39) Kanevskiy, M.; Shur, Y.; Bigelow, N. H.; Bjella, K. L.; Douglas, T. A.; Fortier, D.; Jones, B. M.; Jorgenson, M. T. Yedoma Cryostratigraphy of Recently Excavated Sections of the CRREL Permafrost Tunnel Near Fairbanks, Alaska. *Front. Earth Sci.* **2022**, *9*, No. 758800.
- (40) Kurek, J.; Cwynar, L. C.; Vermaire, J. C. A Late Quaternary Paleotemperature Record from Hanging Lake, Northern Yukon Territory, Eastern Beringia. *Quat. Res.* **2009**, *72*, 246–257.
- (41) Edwards, M. E.; Mock, C. J.; Finney, B. P.; Barber, V. A.; Bartlein, J. Potential Analogues for Paleoclimatic Variations in Eastern Interior Alaska during the Past 14,000 Yr: Atmospheric-Circulation Controls of Regional Temperature and Moisture Responses. *Quat. Sci. Rev.* 2001, 20, 189–202.
- (42) Barber, V. A.; Finney, B. P. Late Quaternary Paleoclimatic Reconstructions for Interior Alaska Based on Paleolake-Level Data and Hydrologic Models.
- (43) Lachniet, M. S.; Lawson, D. E.; Sloat, A. R. Revised ¹⁴ C Dating of Ice Wedge Growth in Interior Alaska (USA) to MIS 2 Reveals Cold Paleoclimate and Carbon Recycling in Ancient Permafrost Terrain. *Quat. Res.* **2012**, *78*, 217–225.
- (44) Douglas, T. A.; Hiemstra, C. A.; Anderson, J. E.; Barbato, R. A.; Bjella, K. L.; Deeb, E. J.; Gelvin, A. B.; Nelsen, P. E.; Newman, S. D.; Saari, S. P.; Wagner, A. M. Recent Degradation of Interior Alaska Permafrost Mappedwith Ground Surveys, Geophysics, Deep Drilling, and Repeatairborne LiDAR. *The Cryosphere* **2021**, *15*, 3555–3575.
- (45) Pienitz, R.; Smol, J. P.; Lean, D. R. S. Physical and Chemical Limnology of 59 Lakes Located between the Southern Yukon and the Tuktoyaktuk Peninsula, Northwest Territories (Canada). *Can. J. Fish. Aquat. Sci.* 1997, 54, 330–346.
- (46) May, N. W.; Axson, J. L.; Watson, A.; Pratt, K. A.; Ault, A. P. Lake Spray Aerosol Generation: A Method for Producing Representative particles from Freshwater Wave Breaking. *Atmos. Meas. Tech.* **2016**, *9*, 4311–4325.
- (47) Philo, L. M.; George, J. C.; Moulton. The Occurrence and Description of Anadromous Fish in the Dease Inlet/Admiralty Bay.
- (48) Hartwell, S. I.; Lomax, T.; Dasher, D. H.; Hoberg, M. K.; Blanchard, A. L.; Jewett, S. Characterization of Benthic Habitats and Contaminant Assessment in Arctic Lagoons and Estuaries. 2018. NOAA Technical Memorandum NOS NCCOS 253. 75 pp. https://doi.org/10.25923/a46e-tm48.
- (49) Goñi, M. A.; Corvi, E. R.; Welch, K. A.; Buktenica, M.; Lebon, K.; Alleau, Y.; Juranek, L. W. Particulate Organic Matter Distributions in Surface Waters of the Pacific Arctic Shelf during the Late Summer and Fall Season. *Mar. Chem.* **2019**, *211*, 75–93.
- (50) Barry, K. R.; Hill, T. C. J.; Jentzsch, C.; Moffett, B. F.; Stratmann, F.; DeMott, P. J. Pragmatic Protocols for Working Cleanly When Measuring Ice Nucleating Particles. *Atmos. Res.* **2021**, 250, No. 105419.
- (51) Uetake, J.; Hill, T. C. J.; Moore, K. A.; DeMott, P. J.; Protat, A.; Kreidenweis, S. M. Airborne Bacteria Confirm the Pristine Nature of the Southern Ocean Boundary Layer. *Proc. Natl. Acad. Sci. U.S.A.* **2020**, *117*, 13275–13282.
- (52) Barry, K. R.; Hill, T. C. J.; Levin, E. J. T.; Twohy, C. H.; Moore, K. A.; Weller, Z. D.; Toohey, D. W.; Reeves, M.; Campos, T.; Geiss, R.; Schill, G. P.; Fischer, E. V.; Kreidenweis, S. M.; DeMott, P. J. Observations of Ice Nucleating Particles in the Free Troposphere From Western US Wildfires. *J. Geophys. Res.: Atmos.* **2021**, 126, No. e2020JD033752.
- (53) DeMott, P. J.; Möhler, O.; Cziczo, D. J.; Hiranuma, N.; Petters, M. D.; Petters, S. S.; Belosi, F.; Bingemer, H. G.; Brooks, S. D.; Budke, C.; Burkert-Kohn, M.; Collier, K. N.; Danielczok, A.; Eppers, O.; Felgitsch, L.; Garimella, S.; Grothe, H.; Herenz, P.; Hill, T. C. J.; Höhler, K.; Kanji, Z. A.; Kiselev, A.; Koop, T.; Kristensen, T. B.; Krüger, K.; Kulkarni, G.; Levin, E. J. T.; Murray, B. J.; Nicosia, A.; O'Sullivan, D.; Peckhaus, A.; Polen, M. J.; Price, H. C.; Reicher, N.; Rothenberg, D. A.; Rudich, Y.; Santachiara, G.; Schiebel, T.; Schrod, J.; Seifried, T. M.; Stratmann, F.; Sullivan, R. C.; Suski, K. J.; Szakáll, M.; Taylor, H. P.; Ullrich, R.; Vergara-Temprado, J.; Wagner, R.; Whale, T. F.; Weber, D.; Welti, A.; Wilson, T. W.; Wolf, M. J.;

- Zenker, J. The Fifth International Workshop on Ice Nucleation Phase 2 (FIN-02): Laboratory Intercomparison of Ice Nucleation Measurements. *Atmos. Meas. Tech.* **2018**, *11*, 6231–6257.
- (54) Vali, G. Quantitative Evaluation of Experimental Results and the Heterogeneous Freezing Nucleation of Super Cooled Liquids. *J. Atmos. Sci.* **1971**, 28, 402–409.
- (55) Agresti, A.; Coull, B. A. Approximate Is Better than "Exact" for Interval Estimation of Binomial Proportions. *Am. Stat.* **1998**, *52*, 119–126.
- (56) Suski, K. J.; Hill, T. C. J.; Levin, E. J. T.; Miller, A.; DeMott, P. J.; Kreidenweis, S. M. Agricultural Harvesting Emissions of Ice-Nucleating Particles. *Atmos. Chem. Phys.* **2018**, *18*, 13755–13771.
- (57) McCluskey, C. S.; Ovadnevaite, J.; Rinaldi, M.; Atkinson, J.; Belosi, F.; Ceburnis, D.; Marullo, S.; Hill, T. C. J.; Lohmann, U.; Kanji, Z. A.; O'Dowd, C.; Kreidenweis, S. M.; DeMott, P. J. Marine and Terrestrial Organic Ice-Nucleating Particles in Pristine Marine to Continentally Influenced Northeast Atlantic Air Masses. *J. Geophys. Res.: Atmos.* 2018, 123, 6196–6212.
- (58) Cruaud, P.; Vigneron, A.; Fradette, M.-S.; Charette, S. J.; Rodriguez, M. J.; Dorea, C. C.; Culley, A. I. Open the Sterivex Casing: An Easy and Effective Way to Improve DNA Extraction Yields: *DNA Extraction from Sterivex* TM Filters. Limnol. Oceanogr.: Methods **2017**, 15, 1015–1020.
- (59) Parada, A. E.; Needham, D. M.; Fuhrman, J. A. Every Base Matters: Assessing Small Subunit RRNA Primers for Marine Microbiomes with Mock Communities, Time Series and Global Field Samples: Primers for Marine Microbiome Studies. *Environ. Microbiol.* 2016, 18, 1403–1414.
- (60) Bolyen, E.; Rideout, J. R.; Dillon, M. R.; Bokulich, N. A.; Abnet, C. C.; Al-Ghalith, G. A.; Alexander, H.; Alm, E. J.; Arumugam, M.; Asnicar, F.; Bai, Y.; Bisanz, J. E.; Bittinger, K.; Brejnrod, A.; Brislawn, C. J.; Brown, C. T.; Callahan, B. J.; Caraballo-Rodríguez, A. M.; Chase, J.; Cope, E. K.; Da Silva, R.; Diener, C.; Dorrestein, P. C.; Douglas, G. M.; Durall, D. M.; Duvallet, C.; Edwardson, C. F.; Ernst, M.; Estaki, M.; Fouquier, J.; Gauglitz, J. M.; Gibbons, S. M.; Gibson, D. L.; Gonzalez, A.; Gorlick, K.; Guo, J.; Hillmann, B.; Holmes, S.; Holste, H.; Huttenhower, C.; Huttley, G. A.; Janssen, S.; Jarmusch, A. K.; Jiang, L.; Kaehler, B. D.; Kang, K. B.; Keefe, C. R.; Keim, P.; Kelley, S. T.; Knights, D.; Koester, I.; Kosciolek, T.; Kreps, J.; Langille, M. G. I.; Lee, J.; Ley, R.; Liu, Y.-X.; Loftfield, E.; Lozupone, C.; Maher, M.; Marotz, C.; Martin, B. D.; McDonald, D.; McIver, L. J.; Melnik, A. V.; Metcalf, J. L.; Morgan, S. C.; Morton, J. T.; Naimey, A. T.; Navas-Molina, J. A.; Nothias, L. F.; Orchanian, S. B.; Pearson, T.; Peoples, S. L.; Petras, D.; Preuss, M. L.; Pruesse, E.; Rasmussen, L. B.; Rivers, A.; Robeson, M. S.; Rosenthal, P.; Segata, N.; Shaffer, M.; Shiffer, A.; Sinha, R.; Song, S. J.; Spear, J. R.; Swafford, A. D.; Thompson, L. R.; Torres, P. J.; Trinh, P.; Tripathi, A.; Turnbaugh, P. J.; Ul-Hasan, S.; van der Hooft, J. J.; Vargas, F.; Vázquez-Baeza, Y.; Vogtmann, E.; von Hippel, M.; Walters, W.; Wan, Y.; Wang, M.; Warren, J.; Weber, K. C.; Williamson, C. H. D.; Willis, A. D.; Xu, Z. Z.; Zaneveld, J. R.; Zhang, Y.; Zhu, Q.; Knight, R.; Caporaso, J. G. Reproducible, Interactive, Scalable and Extensible Microbiome Data Science Using QIIME 2. Nat. Biotechnol. 2019, 37, 852-857.
- (61) Callahan, B. J.; McMurdie, P. J.; Rosen, M. J.; Han, A. W.; Johnson, A. J. A.; Holmes, S. P. DADA2: High-Resolution Sample Inference from Illumina Amplicon Data. *Nat. Methods* **2016**, *13*, 581–583.
- (62) Robeson, M. S.; O'Rourke, D. R.; Kaehler, B. D.; Ziemski, M.; Dillon, M. R.; Foster, J. T.; Bokulich, N. A. RESCRIPt: Reproducible sequence taxonomy reference database management for the masses. *PLoS Comput. Biol.* **2021**, *17* (11), No. e1009581.
- (63) Quast, C.; Pruesse, E.; Yilmaz, P.; Gerken, J.; Schweer, T.; Yarza, P.; Peplies, J.; Glöckner, F. O. The SILVA Ribosomal RNA Gene Database Project: Improved Data Processing and Web-Based Tools. *Nucleic Acids Res.* **2012**, *41*, D590–D596.
- (64) Bokulich, N. A.; Kaehler, B. D.; Rideout, J. R.; Dillon, M.; Bolyen, E.; Knight, R.; Huttley, G. A.; Caporaso, J. Optimizing Taxonomic Classification of Marker-Gene Amplicon Sequences with QIIME 2's Q2-Feature-Classifier Plugin. *Microbiome* **2018**, *6*, No. 90.

- (65) Pedregosa, F.; Varoquaux, G.; Gramfort, A.; Michel, V.; Thirion, B.; Grisel, O.; Blondel, M.; Prettenhofer, P.; Weiss, R.; Dubourg, V.; Vanderplas, J.; Passos, A.; Cournapeau, D. Scikit-Learn: Machine Learning in Python. *J. Mach. Learn. Res.* **2011**, *12*, 2825–2830
- (66) Davis, N. M.; Proctor, D. M.; Holmes, S. P.; Relman, D. A.; Callahan, B. J. Simple Statistical Identification and Removal of Contaminant Sequences in Marker-Gene and Metagenomics Data. *Microbiome* **2018**, *6*, No. 226.
- (67) Jansson, J. K.; Taş, N. The Microbial Ecology of Permafrost. *Nat. Rev. Microbiol.* **2014**, 12, 414–425.
- (68) Shannon, C. E. A Mathematical Theory of Communication; Wiley-IEEE Press, pp 5–83.
- (69) Mackelprang, R.; Burkert, A.; Haw, M.; Mahendrarajah, T.; Conaway, C. H.; Douglas, T. A.; Waldrop, M. P. Microbial Survival Strategies in Ancient Permafrost: Insights from Metagenomics. *ISME J.* 2017, *11*, 2305–2318.
- (70) DeMott, P. J. Quantitative Descriptions of Ice Formation Mechanisms of Silver Iodide, Type Aerosols. *Atmos. Res.* **1995**, 38, 63–99.
- (71) Niemand, M.; Möhler, O.; Vogel, B.; Vogel, H.; Hoose, C.; Connolly, P.; Klein, H.; Bingemer, H.; DeMott, P.; Skrotzki, J.; Leisner, T. A Particle-Surface-Area-Based Parameterization of Immersion Freezing on Desert Dust Particles. *J. Atmos. Sci.* **2012**, 69, 3077–3092.
- (72) DeMott, P. J.; Prenni, A. J.; McMeeking, G. R.; Sullivan, R. C.; Petters, M. D.; Tobo, Y.; Niemand, M.; Möhler, O.; Snider, J. R.; Wang, Z.; Kreidenweis, S. M. Integrating Laboratory and Field Data to Quantify the Immersion Freezing Ice Nucleation Activity of Mineral Dust Particles. *Atmos. Chem. Phys.* **2015**, *15*, 393–409.
- (73) Ullrich, R.; Hoose, C.; Möhler, O.; Niemand, M.; Wagner, R.; Höhler, K.; Hiranuma, N.; Saathoff, H.; Leisner, T. A New Ice Nucleation Active Site Parameterization for Desert Dust and Soot. *J. Atmos. Sci.* **2017**, *74*, 699–717.
- (74) Zinke, J.; Nilsson, E. D.; Zieger, P.; Salter, M. E. The Effect of Seawater Salinity and Seawater Temperature on Sea Salt Aerosol Production. *J. Geophys. Res.: Atmos.* **2022**, *127*, No. e2021JD036005.
- (75) Salter, M. E.; Nilsson, E. D.; Butcher, A.; Bilde, M. On the Seawater Temperature Dependence of the Sea Spray Aerosol Generated by a Continuous Plunging Jet. *J. Geophys. Res.: Atmos.* **2014**, *119*, 9052–9072.
- (76) Shakil, S.; Tank, S. E.; Kokelj, S. V.; Vonk, J. E.; Zolkos, S. Particulate Dominance of Organic Carbon Mobilization from Thaw Slumps on the Peel Plateau, NT: Quantification and Implications for Stream Systems and Permafrost Carbon Release. *Environ. Res. Lett.* **2020**, *15*, No. 114019.
- (77) Kokelj, S. V.; Tunnicliffe, J.; Lacelle, D.; Lantz, T. C.; Chin, K. S.; Fraser, R. Increased Precipitation Drives Mega Slump Development and Destabilization of Ice-Rich Permafrost Terrain, Northwestern Canada. *Global Planet. Change* **2015**, *129*, 56–68.
- (78) Bowden, W. B. Climate Change in the Arctic Permafrost, Thermokarst, and Why They Matter to the Non-Arctic World: Climate Change in the Arctic: Why It Matters. *Geogr. Compass* **2010**, *4*, 1553–1566.
- (79) Nielsen, D. M.; Pieper, P.; Barkhordarian, A.; Overduin, P.; Ilyina, T.; Brovkin, V.; Baehr, J.; Dobrynin, M. Increase in Arctic Coastal Erosion and Its Sensitivity to Warming in the Twenty-First Century. *Nat. Clim. Change* **2022**, *12*, 263–270.
- (80) Kanevskiy, M.; Shur, Y.; Strauss, J.; Jorgenson, T.; Fortier, D.; Stephani, E.; Vasiliev, A. Patterns and Rates of Riverbank Erosion Involving Ice-Rich Permafrost (Yedoma) in Northern Alaska. *Geomorphology* **2016**, 253, 370–384.
- (81) Perkins, R. J.; Gillette, S. M.; Hill, T. C. J.; DeMott, P. J. The Labile Nature of Ice Nucleation by Arizona Test Dust. ACS Earth Space Chem. 2020, 4, 133–141.
- (82) Yang, J. Storm-Driven Mixing and Potential Impact on the Arctic Ocean. J. Geophys. Res. 2004, 109, No. C04008.
- (83) Glacial-Marine Sedimentation; Molnia, B. F., Ed.; Springer: US: Boston, MA, 1983.

(84) Inoue, J.; Tobo, Y.; Taketani, F.; Sato, K. Oceanic Supply of Ice-Nucleating Particles and Its Effect on Ice Cloud Formation: A Case Study in the Arctic Ocean During a Cold-Air Outbreak in Early Winter. *Geophys. Res. Lett.* **2021**, *48*, No. e2021GL094646.

TRecommended by ACS

Does Deep Learning Enhance the Estimation for Spatially Explicit Built Environment Stocks through Nighttime Light Data Set? Evidence from Japanese Metropolitans

Zhiwei Liu, Hiroki Tanikawa, et al.

FEBRUARY 21, 2023

ENVIRONMENTAL SCIENCE & TECHNOLOGY

READ 🗹

Nitrate-Stimulated Release of Naturally Occurring Sedimentary Uranium

Jeffrey P. Westrop, Karrie A. Weber, et al.

FEBRUARY 27, 2023

ENVIRONMENTAL SCIENCE & TECHNOLOGY

READ 🗹

Methane Venting at Cold Heavy Oil Production with Sand (CHOPS) Facilities Is Significantly Underreported and Led by High-Emitting Wells with Low or Negative Value

Simon A. Festa-Bianchet, Matthew R. Johnson, et al.

FEBRUARY 06, 2023

ENVIRONMENTAL SCIENCE & TECHNOLOGY

READ 🗹

Transformations of Ferrihydrite-Extracellular Polymeric Substance Coprecipitates Driven by Dissolved Sulfide: Interrelated Effects of Carbon and Sulfur Loadings

Qihuang Wang, Zimeng Wang, et al.

MARCH 02, 2023

ENVIRONMENTAL SCIENCE & TECHNOLOGY

READ 🗹

Get More Suggestions >